International Journal of Applied Earth Observation and Geoinformation 29 (2014) 11–21

Contents lists available at ScienceDirect

International Journal of Applied Earth Observation and Geoinformation

journal homepage: www.elsevier.com/locate/jag

Ecological site classification of semiarid rangelands: Synergistic use of Landsat and Hyperion imagery

Paula D. Blanco[a,*], Héctor F. del Valle[a], Pablo J. Bouza[a], Graciela I. Metternicht[b], Leonardo A. Hardtke[a]

[a] National Patagonian Center-Argentinean National Research Council, Terrestrial Ecology Unit, Chubut, U9120ACD Puerto Madryn, Chubut, Argentina
[b] Institute of Environmental Studies, University of New South Wales, Sydney 2052, NSW, Australia

ARTICLE INFO

Article history:
Received 10 September 2013
Accepted 20 December 2013

Keywords:
Ecological site
Hyperion
Endmember selection
Mixture tuned matched filtering
Logistic regression
Neural networks
Land management

ABSTRACT

Ecological sites are the basic entity used in rangeland health assessment. This study evaluates the synergistic use of multi- and hyper-spectral satellite imagery for sub-pixel classification of ecological sites in semiarid rangelands. Hyperion and Landsat enhanced thematic mapper (ETM) data are included in a two-step procedure to mapping ecological sites in Patagonian rangelands of Argentina. Firstly, mixture tuned matched filtering and logistic regression analyses are used for Hyperion data processing to obtain ecological site probability images in the area covered by hyperspectral imagery. Secondly, artificial neural networks are applied to model the relationships between the spectral response patterns of Landsat and the probability images from Hyperion, and used to map ecological sites over the entire study area. Overall classification accuracy was 81% (kappa = 0.77) with relatively high accuracies for all ecological sites demonstrating that their spectral signatures are sufficiently distinct to be detectable. Better accuracies were obtained for shrub steppes with desert pavement (producer's and user's accuracies of 89% and 84%, respectively), and shrub-grass steppes associated to tertiary calcareous outcrops (producer's and user's accuracies of 100% and 86%, respectively), while poorer accuracies resulted for shrub-grass steppes on old alluvial plains (producer's and user's accuracies of 75% and 56%, respectively). Fuzzy maps of ecological sites as presented in this research can provide rangeland managers with a tool to stratify the landscape and organize ecological information for rangeland health assessment and monitoring, prioritizing and selecting appropriate management actions, and promoting the recovery of areas degraded in these environments.

1. Introduction

Despite over two decades of remote sensing applications to rangelands assessment, the use of remote sensing imagery for quantitative detection of sparse vegetation, especially in arid and semiarid areas, remains problematic (Dawelbait and Morari, 2008). Previous research has reported on a variety of integration approaches for mapping rangeland vegetation types (Blanco et al., 2009; Bork and Su, 2007; Hill et al., 2005) using a synergy of passive and/or active remote sensors. Image classification conducted on these researches characterised mostly vegetation status (e.g. type, area of coverage, biomass) as a proxy for assessing the state of rangelands, and thus provide value-added information in support of management practices.

During the last years, the rangelands profession has adopted alternative procedures for rangeland evaluation, including state-and-transition models, rangelands health, and the extensive use of individual ecological sites as management units (Briske et al., 2005). An ecological site is a distinctive kind of land with specific soil and physical characteristics that differs from other kinds of land in its ability to produce distinctive types and amounts of vegetation, and in its ability to respond to management actions and natural disturbances. The ES are used to stratify the landscape and organize ecological information for rangeland health assessment and monitoring, so that prioritization and selection of appropriate management actions, and the setting of ecological objectives for management actions is based on site potential (Bestelmeyer and Brown, 2010). Unlike classifications based only on vegetation, ecological site classifications are based on the premise that the differences in plant communities and their resilience are governed by underlying differences in soils, geomorphology, hydrology, and climate (Bestelmeyer et al., 2009).

Karl and Herrick (2010) concur on the usefulness of ecological sites for rangeland monitoring and assessment, highlighting that they also provide a context to support the use of remote sensing techniques in this environment. Despite the identified

* Corresponding author. Tel.: +54 2804504143.
E-mail address: blanco@cenpat.edu.ar (P.D. Blanco).

0303-2434/$ – see front matter © 2013 Elsevier B.V. All rights reserved.
http://dx.doi.org/10.1016/j.jag.2013.12.011

usefulness of the ES classification framework for a remote sensing based assessment and monitoring of rangelands, a research gap exists in the application of satellite-based hyper-spectral imagery for classifying and mapping ecological sites in rangelands. This paper addresses this gap, exploring the value-added information for improved rangelands management that can be generated by a synergistic use of multi- and hyper-spectral satellite imagery using a sub-pixel classification technique. A two-steps methodological framework for data integration was devised using Hyperion and Landsat enhanced thematic mapper (ETM) over a selected pilot area of the Patagonian rangelands of Argentina. Firstly, mixture tuned matched filtering and logistic regression analyses are applied to the extent of the Hyperion hyperspectral imagery to obtain ecological site probability images in the area covered by hyperspectral imagery. Secondly, artificial neural networks (ANN) are applied to model the relationships between the spectral response patterns of Landsat ETM and the probability images from Hyperion, and used to map ecological sites over the entire study area.

2. Remote sensing of rangelands

Previous studies have demonstrated the potential and limitations of remote sensing techniques for practical, rapid, relatively inexpensive and accurate data provision for a variety of rangeland management purposes (Hunt et al., 2003; Palmer and Fortescue, 2004; Mansour et al., 2012). This section reviews some relevant applications of air- and satellite-borne hyperspectral sensors and their combined use with other types of multi-spectral imagery in semi-arid rangeland environments.

2.1. Hyperspectral approaches for mapping rangelands

The availability of operational satellite and airborne hyperspectral sensors (e.g. Hyperion, AVIRIS, DAIS, HyMap), with their narrow (less than 10 nm), near contiguous spectral sampling allow for extraction of detailed spectra signatures for each image pixel throughout visible and shortwave infrared regions of the electromagnetic spectrum (Thenkabail et al., 2004). This high level of spectral detail offers a rich source of compositional information about landscape targets, making it feasible to identify subtle differences between them. Hyperspectral data has proven useful to derive fractional cover of rangeland components including plant species, soil types, litter, bare ground cover types (e.g. surface gravel, stone), and biological soil crusts (Zhang et al., 2008; Rochdi et al., 2008; Liao et al., 2012; Zhang et al., 2013). However, studies conducted at landscape scale tend to be constrained by limited availability of hyper-spectral images over large spatial extents, as these sensors usually collect data along very narrow swaths (e.g. 7.6 km for Hyperion), limiting their ability for landscape scale mapping.

The synergistic use of satellite multi- and hyper-spectral data can help overcome this spatial limitation. Earlier, Okin (2001) used airborne hyper-spectral AVIRIS data over a small area to identify aeolian features and vegetation types in multispectral Landsat imagery covering a large area of arid shrubland in the Mojave Desert. Gumuzzio et al. (2003) were able to synthesized hyperspectral airborne data (DAIS 7915) with multispectral Landsat ETM data to monitor semiarid areas in Central Spain, enabling to extrapolate localized high spectral resolution information to medium spectral resolution data covering a larger area.

2.2. Soft classifiers

Traditional methods of image classification, such as the maximum likelihood classifier and the ISODATA clustering method, assume "pure" or homogeneous pixels (Chuvieco, 2002). These methods are based on the principle of binary logic, in which a pixel is either a full member or not a member of a class, generating hard classifications. However in case of mixed pixel scenarios, common in complex landscapes such as semi-arid rangelands, hard classifications techniques will lead to errors. In these environments the spectral response depends on numerous variables including: (a) vegetation cover by species, (b) total vegetation cover, (c) species or vegetation structure or geometry, (d) leaf geometry, (e) bare ground percentage, (f) amount of shadow, (g) cryptogam cover on the bare soil, (h) lichen cover on soils and rocks, (i) algal mats, (j) microbial desert crusts, (k) gravel and/or pavement, (1) standing dead vegetation, and (m) topography (Tueller, 1995). In semiarid rangelands, soft classifiers based on fuzzy logic or spectral mixture analysis may be more appropriate, as postulated by Cheng et al. (2001). Fuzzy classification techniques assign gradual membership of pixels to thematic classes, measured as degrees in a range from zero to one [0, 1]. This gives the flexibility to represent pixels as entities composed of more than one thematic class.

Linear spectral mixture analysis (LSMA) assumes a model where each pixel spectrum is a linear combination of a finite number of spectrally distinct pure signatures or "endmembers"; subpixel estimates of endmember abundance can be obtained as result (Somers and Asner, 2013; Quintano et al., 2012; McGwire et al., 2000). Spectral mixture analysis has proven useful for providing a spatially and thematically rich description of the distribution of ecological materials in a variety of land cover types with considerable vegetation coverage (e.g., Arsenault and Bonn, 2005; Miao et al., 2006; Tooke et al., 2009). However, lesser success has been obtained when mapping sparsely vegetated landscapes. Alternatively, the method of matched filtering, a partial unmixing technique developed to detect weak spectral signals essentially present in the noise range (Boardman et al., 1995), has been trialed for vegetation and soil distribution mapping in arid and semiarid regions, providing encouraging results (e.g., Lewis, 2001; Okin, 2001; Williams and Hunt, 2002; Yang and Everitt, 2010; Weber and Chen, 2010; Im et al., 2012).

As it is common that matched filtering techniques present false positives for rare materials, Boardman and Kruse (2011) performed a matched filtration tuning (mixture tuned matched filtering, MTMF) that allows more effectively discrimination of "outliers", reducing the number of false positives. MTMF estimates the abundances of user-defined endmembers using partial unmixing. This technique maximizes the response of a known endmember and suppresses the response of the composite unknown background, thus "matching" the known signature. Output from MTMF analysis is a matched filter score image for each endmember, presented as a gray-scale image, which provides a means for estimating the relative degree of match to the reference spectrum.

Image outputs from the MTMF need validation. A confusion matrix is the standard method for validation of classified images (Congalton and Green, 1999), though this approach is less suited to analyze MTMF outputs given that the results are expressed on a continuous scale rather than categorical classes. Therefore, Aspinall (2002) proposed the use of logistic regression for validation of MTMF outputs. Logistic regression uses the sub-pixel estimate that is implicit in the continuous scale matched filter output as the independent data, while the field data remain categorical or continuous (as appropriate to the objects being recorded). Indeed, logistic regression provides an objective function for interpreting the scaling of the matched filter values by transforming them to probability values (scaled from 0 to 1).

2.3. Requirements for sub-pixel classification

Sub-pixel unmixing techniques are typically implemented by first generating a spectral library from which optimal endmembers

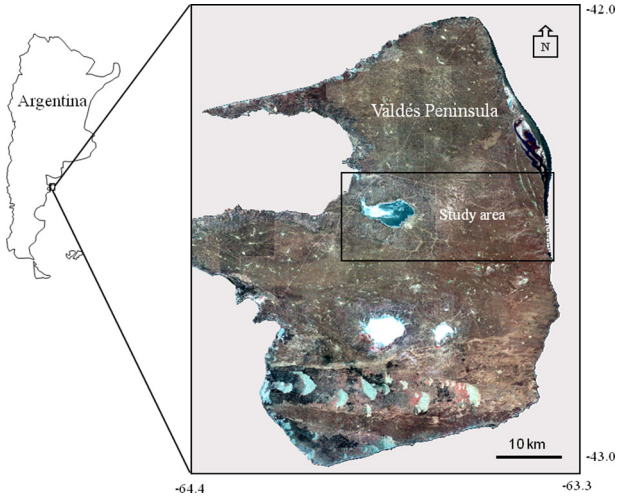

Fig. 1. Study area location.

are selected. One of the most popular techniques to derive pure spectral signatures from the image itself is the pixel purity index (PPI) developed by Boardman (1994) which was designed to search for a set of vertices of a convex geometry in a given image data set that are supposed to represent pure signatures present in the data. However, spectral variations within a single endmember, especially in land cover discrimination, are common due to a variety of environmental factors. To account for this natural variability multiple different approaches to select the optimal number and type of endmembers for a specific scene have been proposed (Somers et al., 2011 provide an extensive review of these techniques). Roberts et al. (1998) introduced a method for selecting endmembers from a spectral library for multiple endmember spectral mixture analysis (MESMA) by using the endmembers that best model the spectral library. In an iterative procedure, based on a spectral library of hundreds of spectra, accounting for each plausible endmember condition, the best-fit model (i.e., lowest RMSE) is assigned to each pixel. Today, this approach is by far the most widely used for selecting representative endmembers. MESMA has been successfully tested in natural environments using hyperspectral imagery (e.g., Roberts et al., 1998; Okin et al., 2001; Dennison and Roberts, 2003a,b; Chen and Vierling, 2006; Bedini et al., 2009).

3. Study area and ecological sites description

A study area of ca 400 km^2, centered at approximately 42°25′S and 63°48′W, was selected in the Patagonian rangelands of southern Argentina (Fig. 1). The climate is semiarid, characterized by an annual mean temperature of 13 °C and an average annual rainfall (1912–2002) of 231 mm, with a high mean interannual variation (coefficient of variation 30%; Barros and Rivero, 1982). The geomorphology of the study area comprised old alluvial plains, piedmont, sand sheets, and alluvial channels. On the east area there is a large dried salt lake called Great Salitral and central to the study area there is a burnt area due to a fire occurred in February 2004. The most widespread vegetation communities are shrub and shrub-grass steppes dominated by *Chuquiraga avellanedae* and grassland dominated by *Stipa tenuis* and *Stipa speciosa* (Bertiller et al., 1981). Extensive, continuous sheep grazing for wool production is the main land use of these rangelands. Based on pre-existing physiographic and vegetation maps (Bertiller et al., 1981; Súnico et al., 1996) and observations of the actual situation in the field, vegetation census and soil sampling were performed on 86 sampling sites. Soil data included texture, bulk density, total organic carbon, exchangeable sodium percentage, soil strength, electrical conductivity, soil structure, and gravel content. In order to identify ecological sites canonical correspondence and cluster analyses were performed. Six dominant ecological sites were identified in the study area; these are detailed in Table 1.

4. Methodology

The methodological steps followed for the classification of the ecological sites are shown in Fig. 2 and detailed in the subsequent paragraphs.

4.1. Image pre-processing

Two 220-channel Hyperion scenes at 30 m resolution were obtained on 20 August 2006. A scaling factor of 40 and 80 was applied for the VNIR bands and SWIR bands, respectively. The Hyperion data were spectrally reduced to a subset of 196 bands after removing the zero-value and overlapping bands. Images were then corrected for atmospheric effects and converted to surface reflectance with the fast line-of-sight atmospheric analysis of spectral hypercubes (FLAASH) algorithm (ENVI, 2009). Landsat ETM data, collected on 21 August 2006, were also processed to obtain their radiance and then converted to top-of-atmosphere reflectance values. Both data sets were georeferenced to a universal transverse mercator (Zone 20) and co-registered image-to-image (<0.5 pixel root mean square error) using nearest neighbour interpolation for resampling to avoid the modification of the radiometric values of the pixels.

The Hyperion reflectance images were used as input into the minimum noise fraction (MNF). The output from MNF is an image with the same dimensionality as the input image. On the basis of the eigenvalues (eigenvalues >5) and the spatial information contained in the output MNF transform images, the first four MNF bands were retained for further analysis and noisy bands were rejected.

4.2. Endmember selection

The spectral response of an ecological site is a composite of the spectral responses of the soils, exposed gravels, green vegetation, non-photosynthetic vegetation, and shading due to topography and surface materials. Previous studies using spectral mixture analysis were carried out at a scale fine enough to discriminate individual surface materials and were therefore able to use laboratory and field reference spectra of these materials (e.g. Dennison and Roberts, 2003b; Roberts et al., 1998). This research departs from data that directly represents individual surface materials, by expanding the MTMF methodology to a landscape scale using composite endmembers to capture all of the spectral mixing occurring within a given ecological site. This approach is similar to the image endmember concept postulated by Smith et al. (1990) in that each ecological site endmember is considered to represent a pure ES drawn from the Hyperion imagery. A similar approach was used by Metternicht and Fermont (1998) to characterize land degradation features related to soil erosion in Bolivia, using Landsat TM data; and more recently, Ballantine et al. (2005) to mapping desert landforms in North Africa, where multiple endmember spectral mixture analysis (MESMA) was applied to composite landform endmembers extracted from MODIS mosaic. In this study, endmembers were extracted from Hyperion image using locations that were known to be representative of a given ecological site.

A number of approaches has been proposed to derive the most representative endmember set that best explains all spectral variability in the image with the least number of uncorrelated (or correlated) endmembers (van der Meer and Jia, 2012). In this

Table 1
Ecological site characteristics.

Code	Physiognomy	Dominant species	Dominant soil	Landform
ES1	Shrub-grass steppe	ChA-CoM-StT	Calciargid	Bajada alluvial
ES2	Shrub steppe with desert pavement	ChA	Natrargid	Old alluvial plain
ES3	Shrub-grass steppe	ChA-ChH-PrG-StT-StL	Torriorthents-tertiary outcrops	Piedmont
ES4	Shrub-grass steppe	ChA-ChH-ScP-LyC-StT-StL	Haplocalcid	Old alluvial plain
ES5	Sandy grassland	StT-PiN-PoL	Haplocalcid	Sand sheets
ES6	Grassland	StS-StH	Haplocalcid	Channel fill

Note: Cha: *Chuquiraga avellanedae*, ChH: *Chuquiraga hystrix*, CoM: *Condalia microphylla*, PrG: *Prosopidastrum globosum*, ScP: *Schinus polygamus*, LyC: *Lycium chilense*, StT: *Stipa tenuis*, StL: *Stipa longiglumis*, PiN: *Piptochaetium napostaense*, PoL: *Poa ligularis*, StS: *Stipa speciosa*, StH: *Stipa humilis*.

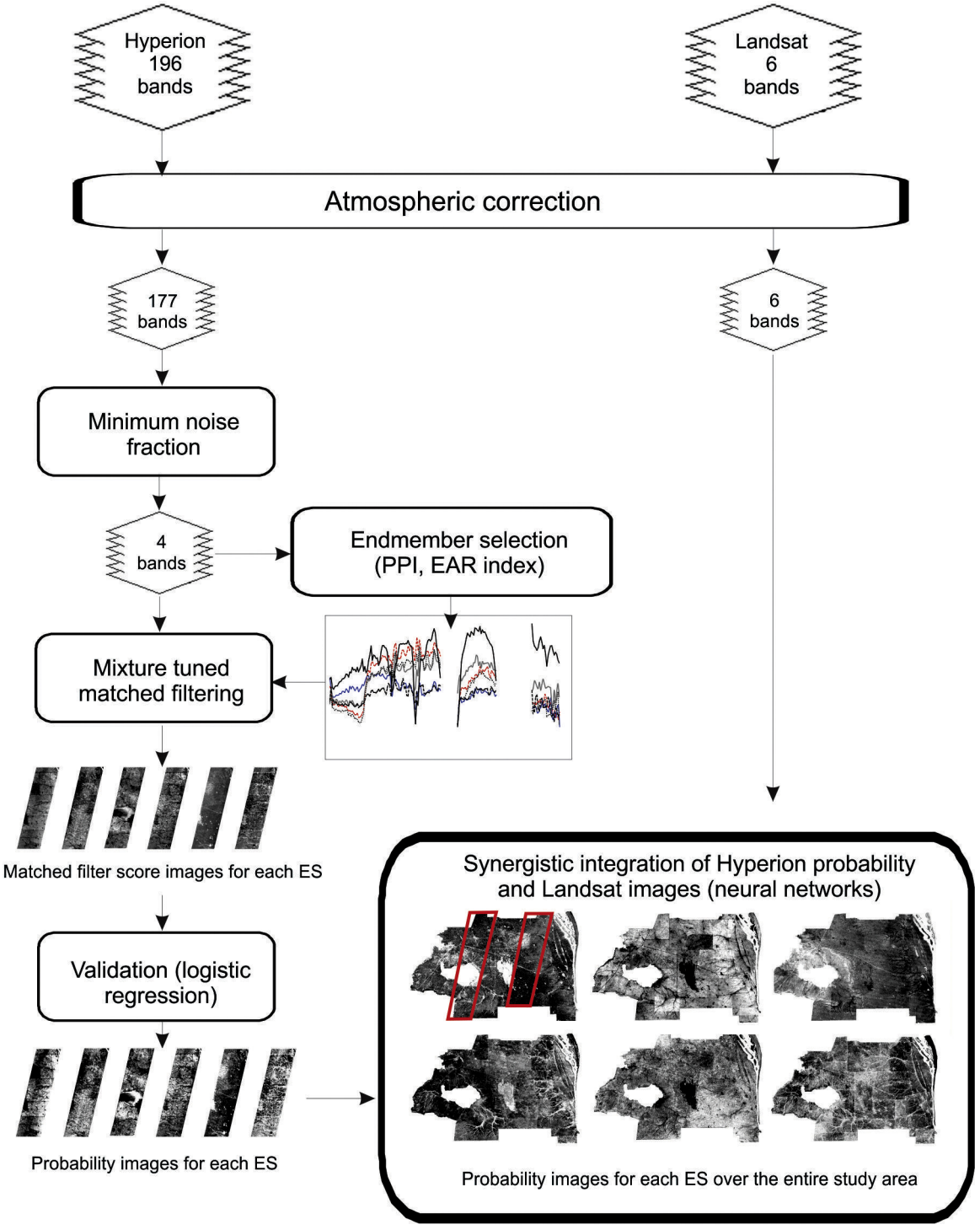

Fig. 2. Flow chart of the methodology adopted for the classification of ecological sites. Red boxes indicateEcological site Hyperion images coverage. Note: RMSE: root mean square error; ES: ecological site. (For interpretation of the references to colour in this figure legend, the reader is referred to the web version of this article.).

research we proposed an endmember selection approach encompassing the three following steps:

1) Using field-based ground reference data, polygons known to be representative of a given ecological site were digitized on Google Earth® imagery, and exported in KLM format;
2) The four MNF transforms from Hyperion imagery were used as input into a Pixel Purity Index (PPI) analysis to identify potential endmembers in the polygons. The output 'pure' pixels from the PPI procedure were examined using multidimensional visualization software (ENVI version 4.8). Additionally, K-means unsupervised clustering and visual examination of pixel spectral signatures were used to organise the spectra of each ecological sites into similar groups. Given the size of the image, and to minimize the computational time of processing, seven pixels were selected for each group for further analysis, obtaining a total of 42 candidate endmembers after this step.
3) To account for the variability within a single endmember, the endmember average RMSE (EAR) method was used for selecting ecological site endmembers (Dennison and Roberts, 2003a). To identify the ecological site spectrum that was most distinct, the spectral library of the 42 endmembers was unmixed by two endmember models of shade and each of the other endmembers in the library. To produce accurate fractions, two constraints were imposed on the mixture decomposition, that the fractions sum up to one and to be nonnegative (Heinz and Chang, 2001). EAR was calculated for each endmember by averaging the RMSE of the set of models that use that endmember to unmix the spectra belonging to the same land cover class:

$$\mathrm{EAR}_{A,A_i} = \frac{\sum_{j=1}^{n} \mathrm{RMSE}_{A_i A_j}}{n-1}$$

where A is the endmember class, A_i is the modeled spectra class, n is the number of spectra in class A, and A_i is the endmember. The term $n-1$ accounts for the endmember modeling itself, which produces a zero RMSE.

4.3. Hyperion image classification

Ecological sites were identified using the MTMF method (Boardman, 1998) applied to the four MNF outputs with the six selected endmembers. Outputs were two floating-point images for each ecological site being mapped. The first output was the matched filter that estimates the degree of match to the reference spectrum and the approximate sub-pixel abundance. The matched filter output has values between 0 and 1.0, where 1.0 indicates a perfect match with the training pixels (also values higher than 1.0 can be obtained, indicating a pixel with a purer spectral signal than those in the training sample). The second output was the infeasibility, measured in noise sigma units, that indicates misclassification in the matched filter result (Boardman, 1998). Correctly mapped pixels have a matched filter score above the background distribution and a low infeasibility value. Pixels with a high matched filter result and high infeasibility are 'false positive' pixels and do not match the target.

Logistic regression was used to relate the MTMF outputs to the field data in order to validate the image classifications, as proposed by Aspinall (2002). Also, logistic regression provides an objective function for interpreting the scaling of the matched filter values by transforming them to probability values (scaled from 0 to 1). Goodness of fit was measured using the Hosmer–Lemeshow test (Hosmer and Lemeshow, 1980), which divides the data into deciles based on the predicted probabilities and computes chi-square from the observed and expected frequencies. The test has 8 degrees of freedom and test the null hypothesis of no difference between the observed and modelled values of the independent variable. In this study, logistic regression uses as the independent variable the sub-pixel estimate that is implicit in the continuous scale matched filter output and as the dependent variable 200 points of occurrence/non-occurrence for each ecological site, which were determined on pansharpened QuickBird images from Google Earth® (Digital Globe catalog IDs 10100100074DCB00-10100100056BEB00, MS 2.4 m/Pan 0.6 m bands) for the area occupied by Hyperion data.

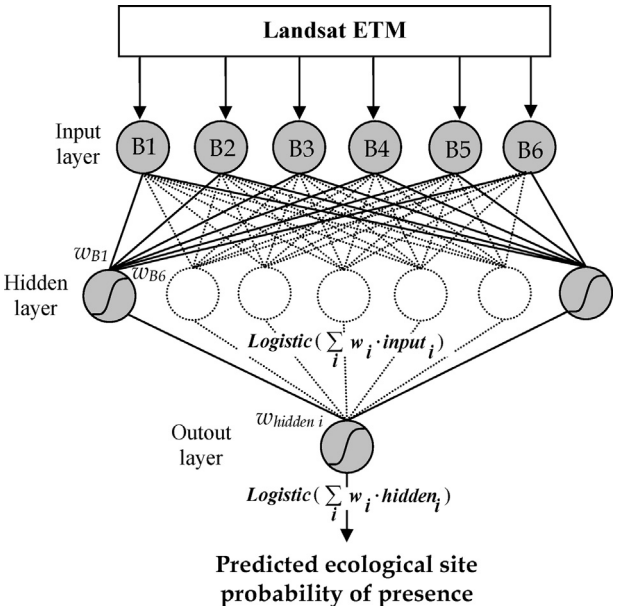

Fig. 3. Architecture of the neural network used to model the relationships between multi- and hyper-spectral data for each ES. Outputs images represent the probability of presence of a particular ES in the study area.

4.4. Synergistic use of Landsat and Hyperion imagery

The research in this paper integrates Hyperion with Landsat ETM data to map ecological sites over the entire study area using artificial neural networks. ANNs have been widely applied to the analysis of remotely sensed data (Mas and Flores, 2008 provide an extensive review). In the context of this study, ANN are relevant to model complex relationships between different data sources, which could be used for predicting the unknown value of a variable (e.g. ecological sites in the Landsat ETM imagery which covers the entire study area) from the known value of another variable (e.g., ecological sites in the Hyperion image covering a sub-set of the study area) in a similar way to regression analysis (Spellman, 1999).

A three Multi-Layered Perceptron (MLP) neural network was generated to model the relationships between the spectral response patterns of the Landsat image and the probability images from Hyperion for each ecological site. The neural network architecture used in this study is shown in Fig. 3. The probability images from Hyperion were used to construct training data for the Landsat imagery. Six input nodes were designed in the neural network to represent the six Landsat bands. One output node was designed for training and generating the probability of presence of a given ecological site. The Multi-Layer Perceptron (MLP) trained with the back-propagation algorithm (BPA), the most frequently used neural network method, was adopted in this study (Gorman and Sejnowski, 1988). A trial-and-error methodology was used to set up the topology for the hidden layer as 12 neurons. In the application, the log-sigmoid transfer function was used and we set learning

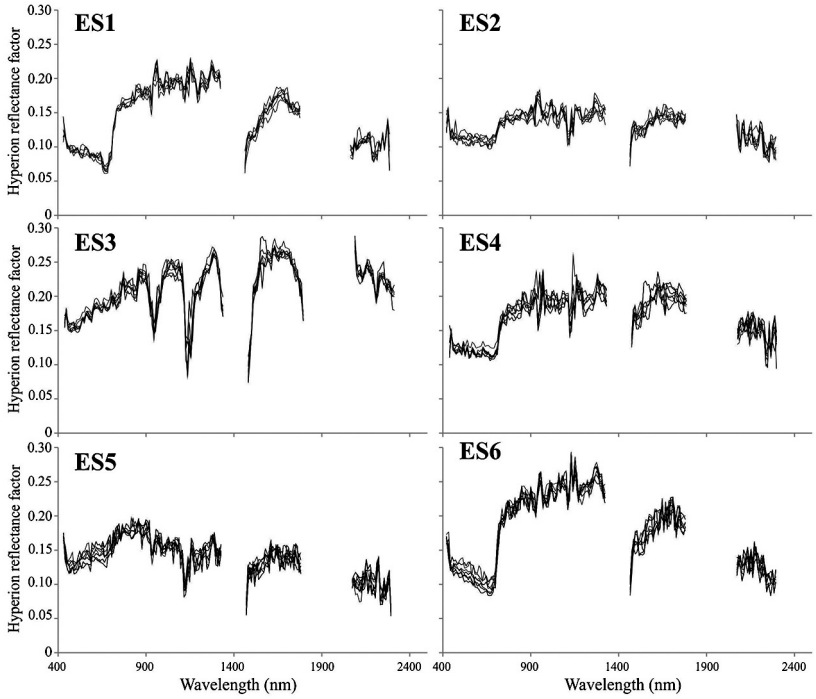

Fig. 4. Spectra of the candidate endmembers being used in the MESMA for each ecological site.

rate to 0.01, momentum to 0.5 and the maximum number of epochs to complete to 10,000.

The pixels of each Hyperion probability image were partitioned into training and validation subsets using the following alternative proportions for each one, respectively: 2/3–1/3, 5/6–1/6, and 8/9–1/9. The training process adjusts the connection weights in order to minimize the root mean square error (RMSE). The RMSE value used in this research for the stopping criterion was set to 0.01. The prediction determination coefficient (R^2_{pred}) between the targets (the probability of presence of a given ecological site) and predicted outputs for each training/validation subset was calculated, selecting the network with greater R^2_{pred}. The relationships modeled by the neural network between multi and hyperspectral data for the portion of study area covered by Hyperion images were used to predict the probability of presence of each ecological site in the rest of the study area. In order to evaluate the performance of the model, the six outputs were integrated in one image where each pixel represents the ecological site with greater probability of occurrence. The prediction map obtained was then compared with independent validation data (ground data, $n = 86$) to determine classification accuracy using confusion matrices with overall, user's, producer's accuracies and Kappa statistic (Congalton, 1991).

5. Results and discussion

5.1. Endmembers selection

EAR was calculated for a total of 42 spectra within 6 ecological sites. Spectra of the 42 candidate endmembers being used in the MESMA are shown in Fig. 4. The endmember with the minimum EAR was selected from each ES. The spectral library of the 42 endmembers was unmixed by each component spectrum and shade, so that a total of 41 unique two endmember models were run for each spectrum. Fig. 5 shows the RMSE image resulting from unmixing the spectral library against itself. The value of brightness in each cell of the matrix indicates the index value of the EAR for the endmember being considered on the *x*-axis, modeling the spectrum that is located on the *y*-axis. Zero values mark the diagonal where a spectrum models itself. The endmember with the lowest rate EAR was considered the most representative of its class and selected for the final stage of classification.

Shrub steppes of *Chuquiraga avellanedae* covering the bajada alluvial and old alluvial plains (ES1 and ES2, respectively) had the lowest EAR value among the six ES, demonstrating the higher within-class spectral homogeneity of these sites. The selected endmembers for these classes had the lowest EAR values ($EAR_{SE1} = 0.9$ and $EAR_{SE2} = 0.7$). Sandy grasslands had the higher minimum EAR values, reflecting higher within-class spectral variability in these disturbed areas (degraded grassland, burnt areas). The selected endmember for this class had the highest EAR value ($EAR_{SE5} = 3.8$). The selected endmembers in shrub-grass steppes and grasslands presented values of EAR index between these extremes ($EAR_{SE3} = 1.9$, $EAR_{SE4} = 1.3$, $EAR_{SE6} = 1.4$).

The spectral signatures of the endmembers for each ecological site selected for using in the MTMF analysis are shown in Fig. 6. Each ES presented different properties of absorption and reflection of electromagnetic radiation related to soil color, parental material and mineralogy, vegetation cover and phenology, position in the landscape and geomorphology (Escadafal et al., 1989; Major et al., 1992). Shrub steppe with desert pavement and high gravel content presented high absorption values (>0.85). Predominant soils in this ES are characterized by the presence of absorbent clay minerals such as smectite, sepiolite and palygorskite (Bouza et al., 2007). These minerals are characterized by the large amount of water that contain in relation to its crystalline structure (in the interlayers of smectites and in the channels of sepiolite and palygorskite) (García-Meléndez et al., 2004), which explains the high absorption values centered in 1400 and 1800 nm for ES2. The presence of calcium carbonate (calcic horizons) in the tertiary marine sediment outcrops present in the pediments (ES3), the clear and bright colors explains the high global reflectance spectrum of ES3. Grasslands with high

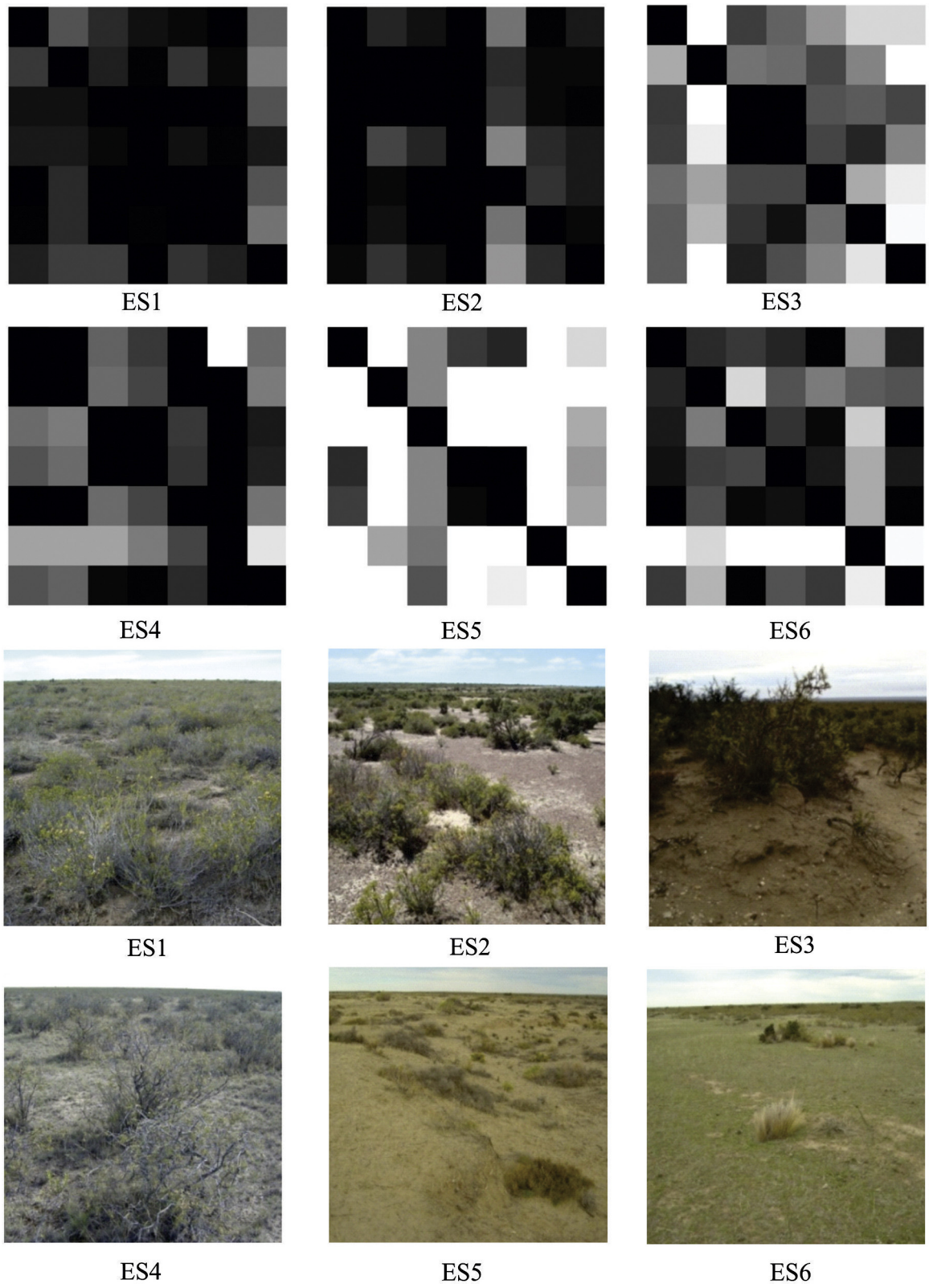

Fig. 5. RMSE image resulting from unmixing the spectral library against itself. Endmember spectra are on the *x*-axis; modeled spectra are on the *y*-axis. The bright bands have higher RMSE values. Zero values denote the diagonal where a spectrum models itself.

herbaceous coverage in channel fills (ES6) had low reflectance in the visible and very high in the near infrared, while grasslands present in disturbed areas (ES5) had a less pronounced variation with low values in the near infrared, evidencing the degradation of the herbaceous cover on this site.

5.2. Fuzzy classification of Hyperion imagery

Matched filter images and logistic regression outputs obtained by applying the MTMF method to the four MNF outputs with the six selected endmembers are shown in Fig. 7. The goodness of fit

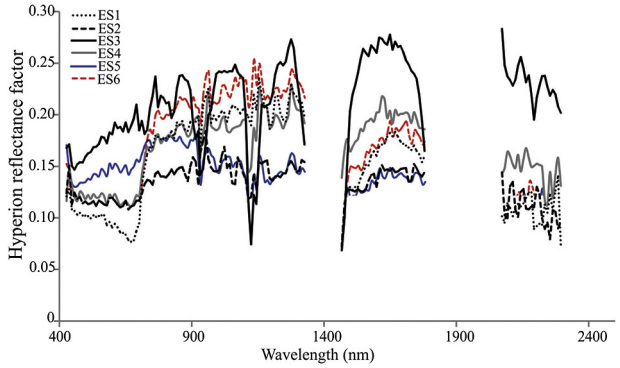

Fig. 6. Spectra of endmembers selected for mixture tuned matched filtering.

between the probability of occurrence of each ES and the independent validation points was analyzed using the Hosmer–Lemeshow test (Hosmer and Lemeshow, 1980). In all cases, the hypothesis of no difference between observed and modeled values of the independent variable was not rejected by the Hosmer–Lemeshow test, demonstrating good agreement between the matched filter scores and the spatial distribution of each ecological site. Shrub-grass steppes associated to tertiary calcareous outcrops (SE3) and shrub steppes with desert pavement (SE2) presented the highest goodness of fit, which is expected considering the distinctive spectral features of these sites (Fig. 6). These results demonstrate the sensitivity of the MTMF analysis for identifying areas with high proportion of calcareous outcrops, as areas with erosion pavements.

Table 2
Performance parameters of the neural networks with greater R^2_{pred} between the probability of presence of a given ecological site and predicted outputs in each ES.

Parameter	ES1	ES2	ES3	ES4	ES6	ES7
$N°p_t$	5/6	2/3	2/3	5/6	5/6	2/3
$N°p_v$	1/6	1/3	1/3	1/6	1/6	1/3
$RMSE_t$	0.0974	0.1112	0.0795	0.1253	0.1137	0.0973
$RMSE_v$	0.0969	0.1013	0.0675	0.1277	0.1040	0.1026
R^2_{pred}	0.87	0.85	0.94	0.75	0.82	0.80

Note: $N°p_t$: number of pixels for training, $N°p_v$: number of pixels for validation, $RMSE_t$: root mean square errors for the training set, $RMSE_v$: root mean square errors for the validation set.

5.3. Synergistic use of Landsat and Hyperion imagery for ecological sites mapping

Table 2 presents the proportions of the training/validation data, RMSE and R^2_{pred} of neural networks which showed the best performance for each ecological site (i.e. the network with greater R^2_{pred} between the probability of presence of a given ecological site and predicted outputs). The predicted R^2_{pred} was acceptable in all cases, showing the highest value (0.94) for pediments with tertiary marine sediment outcrops (ES3). Fig. 8 presents the probability of 'presence images' for each ecological site as modeled by neural networks. These figures show the characteristic spatial patterns of the ecological sites. The presence shrub and shrub-grass steppes are associated with the impact of anthropic activities, a grazing gradient between paddocks being evident. Degraded grasslands, as well as being represented in the burnt area and in the dune on the Great Salitral leeward side, are also associated with a paddock with high grazing pressure history, located in the center of the study area. Conversely, the presence of gullies and tertiary calcareous outcrops

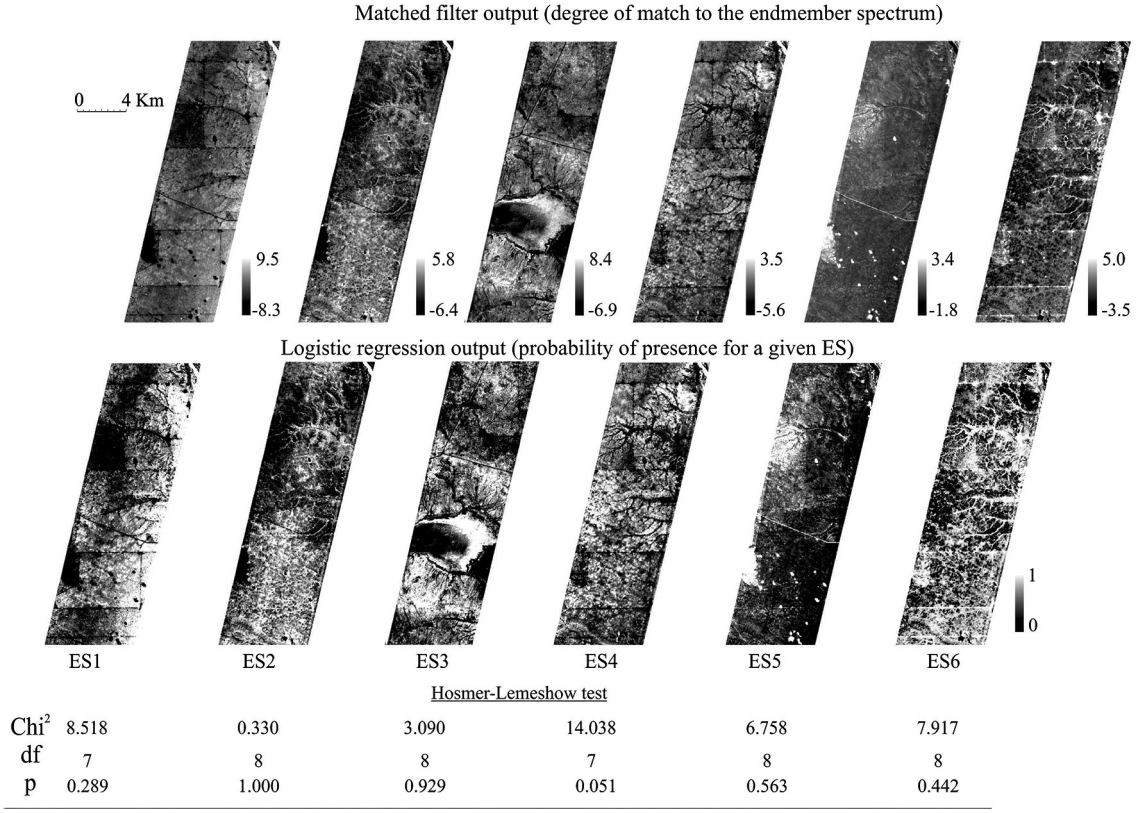

Fig. 7. Results of mixture tuned matched filtering and logistic regression model analysis, and goodness of fit of logistic models of field data for each ES and matched filter output.

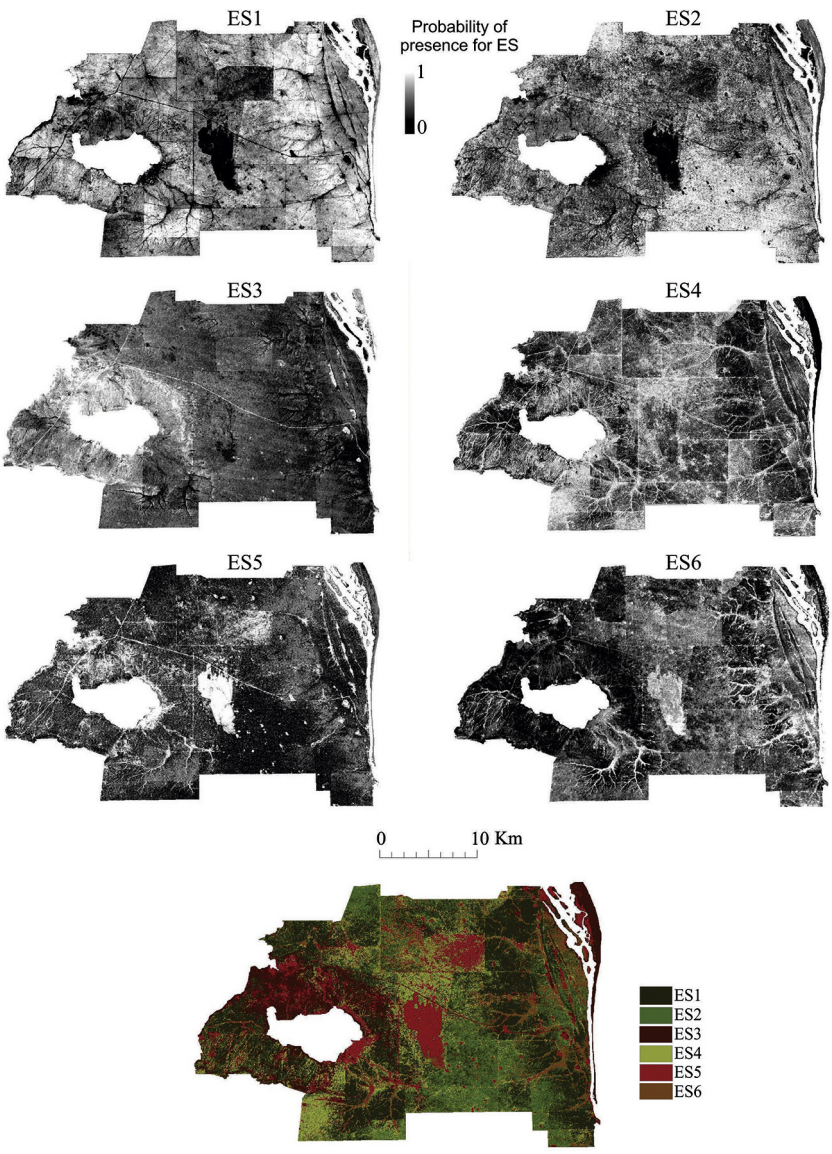

Fig. 8. Probability of 'presence images' of each ecological site as modeled by neural networks in the study area and image output where each pixel represents the ecological site with greater probability of occurrence.

is predominantly associated with the pediments that surround the Great Salitral.

In order to evaluate the performance of the model, the six outputs were integrated in one image where each pixel represents the ecological site with greater probability of occurrence. The prediction map obtained was then compared with independent validation data (ground data, $n = 86$) to determine classification accuracy. The confusion matrix is presented in Table 3; the overall accuracy was 81.0% (kappa = 0.77) with relatively high accuracies for all classes. The lowest user's accuracy (about 56%) was obtained for shrub-grass steppes on the old alluvial plain (ES4) that was mainly confused with shrub-grass steppes on the bajada alluvial (ES1), which in turn decreased the reliability of this class presenting the lowest producer's accuracy (about 72%). By contrast, shrub steppes with desert pavement (ES2) could be accurately discriminated (producer's and user's accuracies of about 89% and 84%, respectively), possibly because of it characteristic spectral signature. The low reflectance of desert pavements is attributed to the dark colouring of clasts and rock fragments (volcanic origin), which cast shadows, trapping more of the incoming sunlight and reducing the amount of reflected energy (Metternicht and Zinck, 1998). Also, producer's and user's accuracies for shrub-grass steppes associated to tertiary calcareous outcrops (SE3) were very high (approximately 100% and 86%, respectively).

5.4. Contributions of remote sensing to the assessment and monitoring of ecological sites in rangelands

Increased remote sensing capabilities have facilitated the development and implementation of dynamic assessment, monitoring, and management systems based on ecological sites for arid and semi-arid rangelands at landscape and regional scales (Maynard et al., 2007; Bestelmeyer et al., 2009; Steele et al., 2012). Fig. 9 illustrates a conceptual framework for organising, synthesizing, and applying knowledge of rangeland ecosystems based on ecological sites, and the potential contribution of current and future remote sensors to that framework. Guided by this framework, this research showed how remote sensing of ecological sites can contribute to facilitating the development of rangeland management strategies. Ecological sites differ in vegetation vigour, species composition and dynamic soil properties in relation to reference conditions (i.e. healthy reference states), the ecosystem services provided,

Table 3
Confusion matrix for the accuracy assessment of the ecological site prediction map (numbers in percentage).

ES prediction map	Ground data						User's accuracy	Commission error
	ES1	ES2	ES3	ES4	ES5	ES6		
ES1	19.05	0	0	2.38	0	0	88.89	11.11
ES2	2.38	19.05	0	1.19	0	0	84.21	15.79
ES3	1.19	1.19	14.29	0	0	0	85.71	14.29
ES4	3.57	1.19	0	10.71	2.38	1.19	56.25	43.75
ES5	0	0	0	0	8.33	2.38	77.78	22.22
ES6	0	0	0	0	0	9.52	88.89	11.11
Producer's accuracy	72.73	88.89	100.00	75.00	77.78	72.73		
Omission error	27.27	11.11	0	25.00	22.22	27.27		

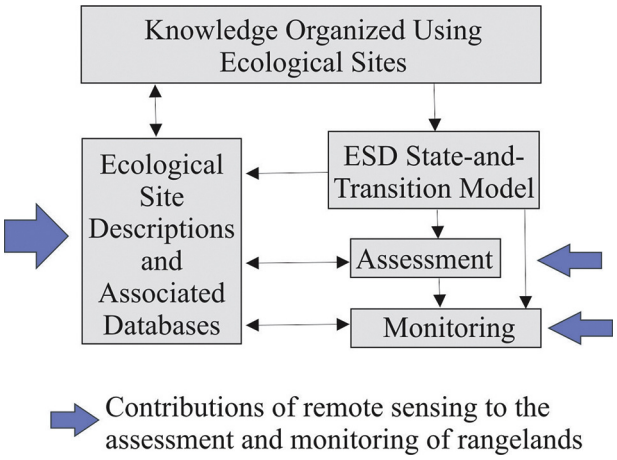

Fig. 9. Conceptual framework for organising, synthesizing, and applying knowledge of rangeland ecosystems based on ecological sites, and the potential contribution of remote sensing to that framework (adapted from Herrick et al., 2006).

and the responses to management and processes of degradation and restoration (USDA-NRCS, 2007). Remote sensing techniques as described in this research can assist in ecological sites composition assessment, providing value-added information for the preparation of site-specific management responses as well as land restoration measures to tackle specific degradation processes. Likewise, synthesis of multi-sensor remote sensing of ecological sites can help identify where monitoring should occur in extensive rangelands like the Argentinean Patagonia, reducing cost and time associated to sampling, while preserving accuracy in information provision related to the status of specific landscapes and associated ecosystem services.

Similar to field-based indicators, remotely-sensed indicators of rangeland ecosystems are of limited utility to management objectives (Karl and Herrick, 2010); whereas remote sensing of ecological sites can provide land managers and decision makers with quantificable and practical management information.

6. Conclusions

The research findings presented in this paper offer a promising environmental application of forthcoming hyperspectral satellite missions like hyperspectral infrared imager (HyspIRI) (http://hyspiri.jpl.nasa.gov/) and hyperspectral imager (HSI) EnMAP (http://www.enmap.org/sensor), set to study the world's ecosystems. Our study shows the potential that HyspIRI and EnMAP could offer to map rangelands ecosystems health (including vegetation types) using the concept of ecological sites, a preferred approach of land managers for prioritising and spatially defining action plans. Likewise, the findings open an avenue for further research on the use of compact high resolution imaging spectrometer CHRIS/PROBA-1 (https://earth.esa.int/web/guest/missions/esa-operational-eo-missions/proba) hyperspectral satellite data to characterise and monitor rangeland environments in the context of sustainable ecosystems management.

The results evidence that hyperspectral data have potential for mapping the distribution of ecological sites in rangelands, and that their synergistic, multi-step use with Landsat imagery as done in this research allows extrapolating local information to regional scale, in a reliable manner. Hyperspectral imagery appears to be an excellent tool for mapping the distribution of ecological sites characterized by shrub and shrub-grass steppes (ES 2 and 3 in Table 1). The presence of gravels of volcanic rocks and tertiary calcareous outcrops provided distinctive absorption spectrums that may be useful in discriminating these ecological sites.

Likewise, fuzzy maps of ecological sites as presented in Fig. 7 can provide a useful input to erosion models, or other modeling applications focused on identifying areas that respond uniformly to hydrological processes. Furthermore, the spectral image resolution of Hyperion is sufficiently fine to evaluate changes in land use/land cover, providing a tool for improved understanding of the influence of anthropogenic activities and ecosystem response. All these potential applications can provide rangeland managers with a tool for planning and monitoring improved use of natural grasslands, and the recovery of areas degraded in these environments.

This research has also demonstrated that a conceptual framework of image classification based on the concept of ecological sites, incorporated into a synergistic model of hyper- and multi-spectral soft classification of remote sensing data can improve classification accuracy of semi-arid rangelands. These results align with previous research findings of Karl and Herrick (2010) who state that digital image classification based on the concept of "ecological sites" can improve classification performance by identifying and isolating areas where soil reflectance is expected to be similar.

Acknowledgments

The Argentinean Space Agency (CONAE) supplied the Hyperion scenes within the framework of a project that promotes monitoring of World Heritage sites (UNESCO). The authors are thankful to the comments received by Prof. Freek van der Meer and an anonymous reviewer, whose views have helped to improve the discussion presented in this paper.

References

Arsenault, É., Bonn, F., 2005. Evaluation of soil erosion protective cover by crop residues using vegetation indices and spectral mixture analysis of multispectral and hyperspectral data. Catena 62 (2–3), 157–172.

Aspinall, R.J., 2002. Use of logistic regression for validation of maps of the spatial distribution of vegetation species derived from high spatial resolution hyperspectral remotely sensed data. Ecol. Model. 157, 301–312.

Ballantine, J.A.C., Okin, G.S., Prentiss, D.E., Roberts, D.A., 2005. Mapping north African landforms using continental-scale unmixing of MODIS imagery. Remote Sens. Environ. 47, 470–483.

Barros, V., Rivero, M.M., 1982. Mapas de Probabilidad de Precipitación en la Provincia del Chubut, Contribución N° 54. CENPAT-CONICET, Chubut, Argentina.

Bedini, E., van der Meer, F., van Ruitenbeek, F., 2009. Use of HyMap imaging spectrometer data to map mineralogy in the Rodalquilar caldera, southeast Spain. Int. J. Remote Sens. 30, 327–348.

Bertiller, M.B., Beeskow, A.M., Irisarri, M.P., 1981. Caracteres Fisonómicos y Florísticos de Vegetación del Chubut: 2. La Península Valdés y el Istmo Ameghino, Contribución N° 41. CENPAT-CONICET, Chubut, Argentina.

Bestelmeyer, B.T., Tugel, A.J., Peacock, G.L., Robinett, D.G., Shaver, P.L., Brown, J.R., Herrick, J.E., Sanchez, H., Havstad, K.M., 2009. State-and-transition models for heterogeneous landscapes: astrategy for development and application. Rangeland Ecol. Manag. 62 (1), 1–15.

Bestelmeyer, B.T., Brown, J.R., 2010. An introduction to the special issue on ecological sites. Rangelands 32, 3–4.

Blanco, P.D., Metternicht, G.I., del Valle, H.F., 2009. Improving the discrimination of vegetation and landforms patterns in sandy rangelands: a synergistic approach. Int. J. Remote Sens. 30, 2579–2605.

Boardman, J.W., Kruse, F.A., 2011. Analysis of imaging spectrometer data using N-dimensional geometry and a mixture-tuned matched filtering approach. IEEE Trans. Geosci. Remote Sens. 49, 4138–4152.

Boardman, J.W., 1994. Geometric mixture analysis of imaging spectrometry data. Proc. Int. Geosci. Remote Sens. Symp. 4, 2369–2371.

Boardman, J.W., Kruse, F.A., Green, R.O., 1995. Mapping target signatures via partial unmixing of AVIRIS data. In: Summaries of the Fifth Annual JPL Airborne Geoscience Workshop, Jet Propulsion Laboratory, Pasadena, CA, 24–26 January, pp. 23–26.

Bork, E.W., Su, J.G., 2007. Integrating LIDAR data and multispectral imagery for enhanced classification of rangeland vegetation: a meta analysis. Remote Sens. Environ. 111, 11–24.

Bouza, P.J., Simón, M., Aguilar, J., del Valle, H., Rostagno, M., 2007. Fibrous-clay mineral formation and soil evolution in Aridisols of northeastern Patagonia, Argentina. Geoderma 139 (1–2), 38–50.

Briske, D.D., Fuhlendorf, S.D., Smeins, F.E., 2005. State-and-transition models, thresholds, and rangeland health: a synthesis of ecological concepts and perspectives. Rangeland Ecol. Manag. 58, 1–10.

Chen, X., Vierling, L., 2006. Spectral mixture analysis of hyperspectral data acquired using a tethered balloon. Remote Sens. Environ. 103, 338–350.

Cheng, T., Molenaar, M., Lin, H., 2001. Formalizing fuzzy objects from uncertain classification results. Int. J. Geogr. Inf. Sci. 15 (1), 27–42.

Chuvieco, E., 2002. Teledetección Ambiental. La observación de la tierra desde el espacio. Ariel Ciencia, Barcelona, España.

Congalton, R., 1991. A review of assessing the accuracy of classifications of remotely sensed data. Remote Sens. Environ. 37, 35–46.

Congalton, R.G., Green, K., 1999. Assessing The Accuracy of Remotely Sense Data: Principles and Practices. Lewis Publishers, New York.

Dawelbait, M., Morari, F., 2008. Limits and potentialities of studying dryland vegetation using the optical remote sensing. Ital. J. Agron. 2, 97–106.

Dennison, P.E., Roberts, D.A., 2003a. Endmember selection for multiple endmember spectral mixture analysis using endmember average RMSE. Remote Sens. Environ. 87, 123–135.

Dennison, P.E., Roberts, D.A., 2003b. The effects of vegetation phenology on endmember selection and species mapping in Southern California Chaparral. Remote Sens. Environ. 87, 123–135.

ENVI, 2009. Atmospheric Correction Module: QUAC and FLAASH User' Guide. Exelis Visual Information Solutions, Boulder, CO.

Escadafal, R., Girard, M.C., Courault, D., 1989. Munsell soil color and soil reflectance in the visible spectral bands of Landsat MSS and TM data. Remote Sens. Environ. 27, 37–46.

García-Meléndez, E., Ferrer-Juliá, M., Bermejo, A., Suárez, M., 2004. Relación entre la respuesta espectral (visible -Infrarrojo cercano) y la composición mineralógica de materiales sedimentarios del borde occidental de la Cuenca del duero. Revista de la Sociedad Geológica de España 17, 39–47.

Gorman, R.P., Sejnowski, T.J., 1988. Learned classification of sonar targets using a massively parallel network. IEEE Trans. Acoust. Speech Sig. Proc. 36, 1135–1140.

Gumuzzio, J., Schmid, T., Koch, M., Mather, P., Rodríguez, M., 2003. Synergetic use of multispectral and hyperspectral data in characterising changes in semiarid wetlands in Spain. In: Proceeding of 3rd EARSeL Workshop on Imaging Spectroscopy, Oberpfaffenhofen, 13–16 (on CDROM).

Heinz, D.C., Chang, C.I., 2001. Fully constrained least square linear spectral mixture analysis method for material quantification in hyperspectral imagery. IEEE Trans. Geosci. Remote Sens. 39, 529–545.

Hill, M.J., Ticehurst, C.-I., Lee, J.-S., Grunes, M.R., et al., 2005. Integration of optical and radar classifications for mapping pasture type in Western Australia. IEEE Trans. Geosci. Remote Sens. 43, 1665–1681.

Hosmer, D.W., Lemeshow, S., 1980. A goodness-of-fit test for the multiple logistic regression model. Commun. Stat. A10, 1043–1069.

Hunt E.R. Jr., Everitt, J., Ritchie, J., Moran, M., Booth, D., Anderson, G., Clark, P., Seyfried, P., 2003. Applications and research using remote sensing for rangeland management. Photogramm. Eng. Rem. Sens. 69 (6), 675–693.

Im, J., Jensen, J.R., Jensen, R.R., Gladden, J., Waugh, J., Serrato, M., 2012. Vegetation cover analysis of hazardous waste sites in Utah and Arizona using hyperspectral remote sensing. Remote Sens. 4, 327–353.

Karl, J., Herrick, J., 2010. Monitoring and assessment based on ecological sites. Rangelands 32 (6), 60–64.

Lewis, M.M., 2001. Mapping arid landscapes with multispectral and hyperspectral imagery. In: Proceeding of the Geoscience and Remote Sensing Symposium, 6, IGARSS '01, IEEE, Sydney, NSW, Australia, pp. 2902–2904.

Liao, C., Zhang, X., Bao, H., 2012. Estimation of fractional vegetation cover by unmixing HJ-1 satellite hyperspectral data. In: Proceeding of Second International Workshop on Earth Observation and Remote Sensing Applications.

Major, D., Janzen, H., Olson, B., McGinn, S., 1992. Reflectance characteristic of Southern Alberta soils. Can. J. Soil Sci. 72, 611–615.

Mansour, K., Mutanga, O., Everson, T., 2012. Remote sensing based indicators of vegetation species for assessing rangeland degradation: opportunities and challenges. Afr.J. Agric. Res. 7 (22), 3261–3270.

Mas, J., Flores, J., 2008. The application of artificial neural networks to the analysis of remotely sensed data. Int. J. Remote Sens. 29 (3), 617–663.

Maynard, C., Lawrence, R., Nielsen, G., Decker, G., 2007. Ecological site descriptions and remotely sensed imagery as a tool for rangeland evaluation. Can. J. Remote Sens. 33 (2), 109–115.

McGwire, K., Minor, T., Fenstermaker, L., 2000. Hyperspectral mixture modeling for quantifying sparse vegetation cover in arid environments. Remote Sens. Environ. 72, 360–374.

Metternicht, G.I., Fermont, A., 1998. Estimating erosion surface features by linear mixture modeling. Remote Sens. Environ. 64, 254–265.

Metternicht, G.I., Zinck, J.A., 1998. Evaluating the information content of JERS-1 SAR and Landsat TM data for discrimination of soil erosion features. ISPRS J. Photogramm. Rem. Sens. 53, 143–153.

Miao, X., Gong, P., Swope, S., Pu, R., Carruthers, R., Anderson, G.L., Heaton, J.S., Tracy, C.R., 2006. Estimation of yellow starthistle abundance through CASI-2 hyperspectral imagery using linear spectral mixture models. Remote Sens. Environ. 101 (3), 329–341.

Okin, G., Murray, B., Schlesinger, W.H., 2001. Degradation of sandy arid shrubland environments: observations, process modelling, and management implications. J. Arid Environ. 47, 123–144.

Palmer, A., Fortescue, A., 2004. Remote sensing and change detection in rangelands. Afr. J. Range For. Sci. 21 (2), 123–128.

Quintano, C., Fernández-Mansob, A., Shimabukuroc, Y.E., Pereirac, G., 2012. Multiple endmember spectral mixture analysis (MESMA) to map burn levels from Landsat in Mediterranean countries. Int. J. Remote Sens. 33, 5307–5340.

Roberts, D.A., Gardner, M., Church, R., Ustin, S., Scheer, G., Green, R.O., 1998. Mapping chaparral in the Santa Monica Mountains using multiple endmember spectral mixture models. Remote Sens. Environ. 65, 267–279.

Rochdi, N., Eddy, P., Staenz, K., Zhang, J., Lutz, C., 2008. Rangeland monitoring using hyperspectral remote sensing data and spectral mixture analysis. In: Proceeding of SPIE 7110, Remote Sensing for Environmental Monitoring, GIS Applications, and Geology VIII, 711023, 14 October.

Smith, M.O., Ustin, S.L., Adams, J.B., Gillespie, A.R., 1990. Vegetation in deserts: I. A regional measure of abundance from multispectral images. Remote Sens. Environ. 31, 1–26.

Somers, B., Asner, G.P., 2013. Multi-temporal hyperspectral mixture analysis and feature selection for invasive species mapping in rainforests. Remote Sens. Environ. 136, 14–27.

Somers, B., Asner, G., Tits, L., Coppin, P., 2011. Endmember variability in spectral mixture analysis: a review. Remote Sens. Environ. 115, 1603–1616.

Spellman, G., 1999. An application of artificial neural networks to the prediction of surface ozone concentration in the United Kingdom. Appl. Geogr. 19, 123–136.

Steele, C.M., Bestelmeyer, B.T., Smith, P.L., Yanoff, S., Burkett, L.M., 2012. Spatially-explicit representation of state-and-transition models. Rangeland Ecol. Manag. 65, 213–222.

Súnico, A., Bouza, P., del Valle, H.F., 1996. Erosion of subsurface horizons in northeastern Patagonia, Argentina. Arid Soil Res. Rehab. 10, 359–378.

Thenkabail, P., Enclona, E., Ashton, M., Van Der Meer, B., 2004. Accuracy assessments of hyperspectral waveband performance for vegetation analysis applications. Remote Sens. Environ. 91 (3-4), 354–376.

Tooke, T., Coops, N., Goodwin, N., Voogt, J., 2009. Extracting urban vegetation characteristics using spectral mixture analysis and decision tree classifications. Remote Sens. Environ. 113 (2), 398–407.

Tueller, P.T., 1995. Remote sensing in the management of rangelands. Ann. Arid Zone 34, 191–207.

USDA-NRCS, 2007. US Department of Agriculture-Natural Resources Conservation Service. National Soil Survey Handbook, title 430-VI, http://soils.usda.gov/technical/handbook/ (Accesed 3 September, 2013).

Van der Meer, F.D., Jia, X., 2012. Collinearity and orthogonality of endmembers in linear spectral unmixing. Int. J. Appl. Earth Obs. Geoinform. 18, 491–503.

Weber, K.T., Chen, F., 2010. Detection thresholds for rare, spectrally unique targets within semiarid rangelands. Photogramm. Eng. Rem. Sens. 76 (11), 1253–1259.

Williams, A.P., Hunt Jr., E.R., 2002. Estimation of leafy spurge cover from hyperspectral imagery using mixture tuned matched filtering. Remote Sens. Environ. 82, 446–456.

Yang, C., Everitt, J.H., 2010. Mapping three invasive weeds using airborne hyperspectral imagery. Ecol. Inform. 5 (5), 429–439.

Zhang, J., Staenz, K., Eddy, P.R., Rochdi, N., Rolfson, D., Smith, A., 2008. Analysis of spaceborne hyperion imagery for the estimation of fractional cover of rangeland ecosystems. International archives of the photogrammetry. Remote Sens. Spat. Inform. Sci. 36 (Part B7), on CD-ROM.

Zhang, X., Liao, C., Li, J., Sun, Q., 2013. Fractional vegetation cover estimation in arid and semi-arid environments using HJ-1 satellite hyperspectral data. Int. J. Appl. Earth Obs. Geoinform. 21, 506–512.